Heliyon 10 (2024) e35344

Contents lists available at ScienceDirect

Heliyon

journal homepage: www.cell.com/heliyon

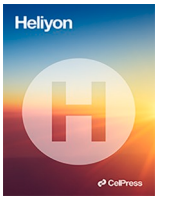

Research article

Predicting progression-free survival in patients with epithelial ovarian cancer using an interpretable random forest model

Lian Jian [a,1], Xiaoyan Chen [b,1], Pingsheng Hu [a,1], Handong Li [a], Chao Fang [c], Jing Wang [c], Nayiyuan Wu [d,**], Xiaoping Yu [a,*]

[a] *Department of Radiology, The Affiliated Cancer Hospital of Xiangya School of Medicine, Central South University/Hunan Cancer Hospital, Changsha, Hunan, China*
[b] *Department of Pathology, The Affiliated Cancer Hospital of Xiangya School of Medicine, Central South University/Hunan Cancer Hospital, Changsha, Hunan, China*
[c] *Department of Clinical Pharmaceutical Research Institution, The Affiliated Cancer Hospital of Xiangya School of Medicine, Central South University/Hunan Cancer Hospital, Changsha, Hunan, China*
[d] *Central Laboratory, The Affiliated Cancer Hospital of Xiangya School of Medicine, Central South University/Hunan Cancer Hospital, Changsha, Hunan, China*

ARTICLE INFO

Keywords:
Ovarian cancer
Computed tomography
Radiomics
Random forest
Prognosis

ABSTRACT

Prognostic models play a crucial role in providing personalised risk assessment, guiding treatment decisions, and facilitating the counselling of patients with cancer. However, previous imaging-based artificial intelligence models of epithelial ovarian cancer lacked interpretability. In this study, we aimed to develop an interpretable machine-learning model to predict progression-free survival in patients with epithelial ovarian cancer using clinical variables and radiomics features. A total of 102 patients with epithelial ovarian cancer who underwent contrast-enhanced computed tomography scans were enrolled in this retrospective study. Pre-surgery clinical data, including age, performance status, body mass index, tumour stage, venous blood cancer antigen-125 (CA125) level, white blood cell count, neutrophil count, red blood cell count, haemoglobin level, and platelet count, were obtained from medical records. The volume of interest for each tumour was manually delineated slice-by-slice along the boundary. A total of 2074 radiomic features were extracted from the pre- and post-contrast computed tomography images. Optimal radiomic features were selected using the Least Absolute Shrinkage and Selection Operator logistic regression. Multivariate Cox analysis was performed to identify independent predictors of three-year progression-free survival. The random forest algorithm developed radiomic and combined models using four-fold cross-validation. Finally, the Shapley additive explanation algorithm was applied to interpret the predictions of the combined model. Multivariate Cox analysis identified CA-125 levels ($P = 0.015$), tumour stage ($P = 0.019$), and Radscore ($P < 0.001$) as independent predictors of progression-free survival. The combined model based on these factors achieved an area under the curve of 0.812 (95 % confidence interval: 0.802–0.822) in the training cohort and 0.772 (95 % confidence interval: 0.727–0.817) in the validation cohort. The most impactful features on the model output were Radscore, followed by tumour stage and

* Corresponding author. No.283, TongzipoRoad, Changsha 410013, China.
** Corresponding author. No.283, TongzipoRoad, Changsha 410013, China.
E-mail addresses: wunayiyuan@163.com (N. Wu), yuxiaoping@hnca.org.cn (X. Yu).
[1] Lian Jian, Xiaoyan Chen, and Pingsheng Hu contributed equally to this work.

https://doi.org/10.1016/j.heliyon.2024.e35344
Received 18 February 2024; Received in revised form 26 July 2024; Accepted 26 July 2024
Available online 26 July 2024
2405-8440/© 2024 The Authors. Published by Elsevier Ltd. This is an open access article under the CC BY-NC-ND license (http://creativecommons.org/licenses/by-nc-nd/4.0/).

CA-125. In conclusion, the Shapley additive explanation-based interpretation of the prognostic model enables clinicians to understand the reasoning behind predictions better.

1. Introduction

Epithelial ovarian cancer (EOC) is the fifth leading cause of cancer-related deaths in women [1]. Despite advancements in treatment strategies, the prognosis of EOC remains challenging, primarily due to late-stage diagnosis and high rates of recurrence [2]. Thus, there is an urgent need for accurate prognostic tools that can aid treatment planning and improve patient outcomes.

Preoperative medical imaging is pivotal in EOC management and offers valuable insight beyond human visual interpretation [3]. Radiomics, a rapidly evolving field of medical imaging, holds great promise for cancer research [4]. Radiomics involves high-throughput extraction of quantitative imaging features from medical images, enabling the conversion of medical images into mineable data [5]. These features capture the heterogeneity and spatial characteristics of tumours and provide valuable information on tumour biology and behaviour [6]. Recently, radiomics has gained significant attention in multiple clinical scenarios of EOC, including precise diagnosis, pathological classification, targeted biopsy guidance, and prognostic prediction [7]. Radiomics has the potential to identify hidden prognostic markers and facilitate personalised treatment strategies by extracting numerous quantitative features from imaging modalities, such as contrast-enhanced computed tomography (CECT), magnetic resonance imaging (MRI), and positron emission tomography (PET), radiomics has the potential to uncover hidden prognostic markers and facilitate personalised treatment strategies.

The primary purpose of our study was to investigate the utility of imaging-based radiomics in predicting survival outcomes in patients with EOC. By leveraging the rich information embedded in medical images, we developed a radiomics-based model that can accurately stratify patients based on their survival outcomes. Such a machine-learning model could serve as a valuable tool for clinicians in risk assessment, treatment planning, and monitoring disease progression. Moreover, we explored the potential synergistic effects of combining radiomics features with clinical data. By integrating radiomic features with traditional clinical factors, the predictive power of our machine-learning model can be enhanced. The integration of radiomics into EOC research has the potential to revolutionise prognostic assessment and improve patient outcomes. By unlocking hidden information within medical images, radiomics can provide valuable insights into tumour behaviour and facilitate personalised treatment strategies. Additionally, a Shapley additive explanation (SHAP) technique was used to explain the predictions generated by the clinical radiomic model [8]. This study contributes to the growing body of evidence supporting using interpretable radiomics-based machine learning models in EOC survival prediction, ultimately paving the way for more effective and individualised patient care.

2. Materials and methods

2.1. Patients

This retrospective study was approved by the Institutional Ethics Review Board (approval number: 202475), which waived the requirement for informed consent. Consecutive patients with EOC who underwent surgery in our cancer-specialised hospital between June 1, 2013 and December 31, 2015 were reviewed. The cutofff date for survival data statistics was August 31, 2021. The inclusion criteria were as follows [1]: histologically confirmed EOC [2], available pretreatment CECT images [3], no prior anticancer treatment received before baseline CECT, and [4] patients who underwent surgical cytoreduction. Patients who had incomplete clinical data did

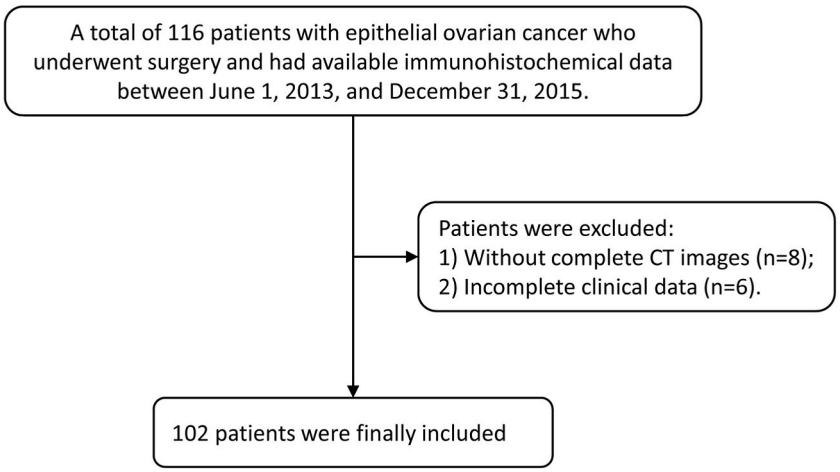

Fig. 1. The flowchart of patients' enrollment.

not undergo preoperative computed tomography (CT) scans, lacked CECT images, or had no available pathological information were excluded. Finally, 102 patients were included in this study. Fig. 1 illustrates the pathways for patient inclusion and exclusion. Clinical data, including age, body mass index (BMI), International Federation of Gynecology and Obstetrics (FIGO) stage, white blood cell count, neutrophil count, red blood count, haemoglobin level, platelet count, venous blood cancer antigen 125 (CA125) level, whole blood CA125 level, and treatment regimens were retrieved from electronic medical records. The missing values were imputed using the random forest (RF) imputation method [9]. The endpoint was progression-free survival (PFS), the interval from the treatment date to disease progression or death.

2.2. Radiomic analysis pipeline

2.2.1. CT image acquisitions

Fig. 2a–d illustrates the overall study design. CT scans were performed using a 64-row CT scanner (Somatom definition AS large-aperture, Siemens Healthcare). The scanning parameters were as follows: tube voltage of 120-kVp, tube current of 252-mAs; field of view, 384 × 384 mm^2; detector width, 38.4 mm, gantry rotation time, 0.5 s, beam pitch 0.6, and slice thickness, 5 mm. Iohexol (350 mg I/ml) was administered via the elbow vein at a rate of 2.5–3.0 ml/s.

2.2.2. Tumor segmentation

The CT images (Fig. 3a and b) were manually segmented using open-source software ITK-SNAP 3.6.0 (www.itksnap.org). Segmentation of the images was performed separately for each phase (pre- and post-contrast) by a radiologist specialising in gynaecological oncology with six years of experience. The segmentation results were reviewed by a board-certified radiologist with more than 10 years of experience. All readers or assessors were blinded to patients' clinical information and pathological results. If there were any discrepancies during image reading or tumor segmentation, a group discussion was conducted to achieve a consensus.

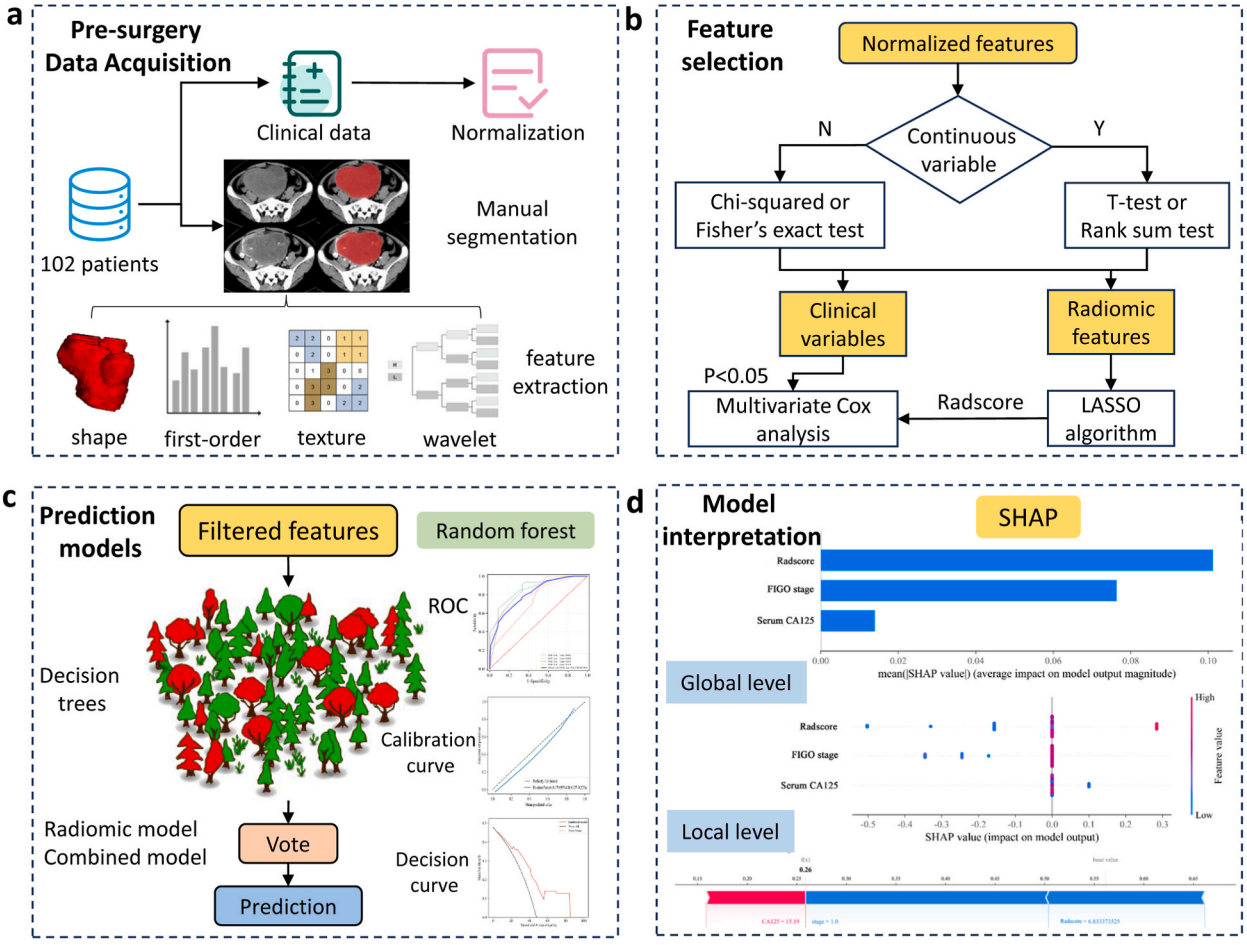

Fig. 2. The overall design of this study. The main steps include (a) data acquisition; (b) feature selection; (c) predictive model development; (d) model interpretation.

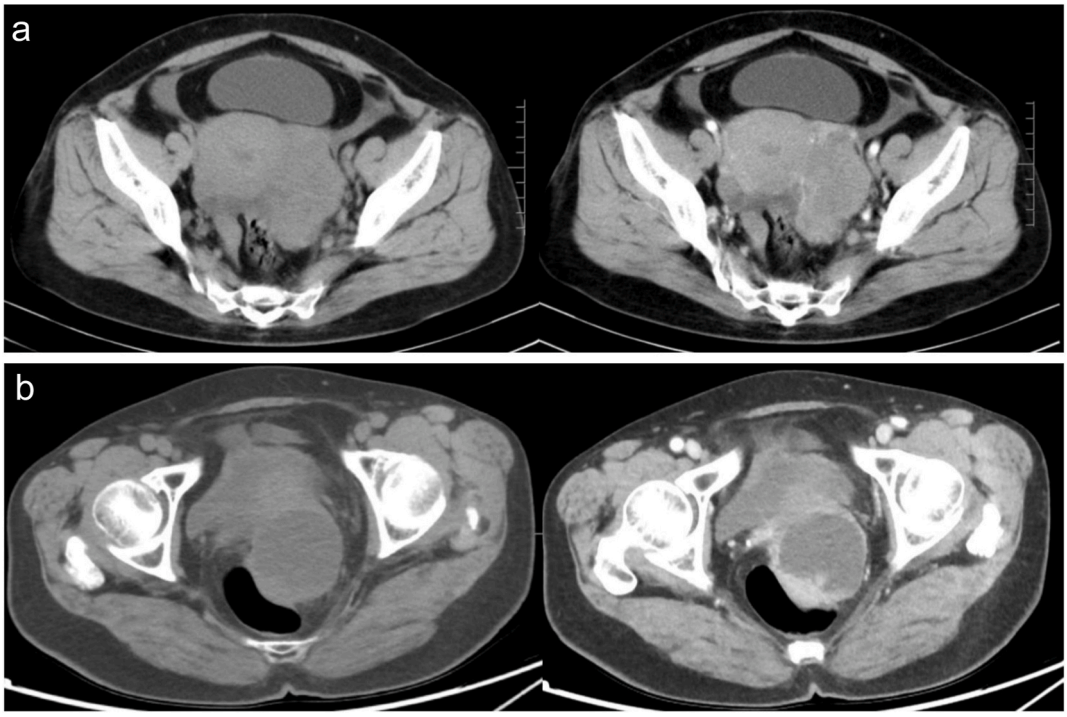

Fig. 3. Two representative cases of pre- and post-contrast CT images. (a) A 41-year-old female patient presented with a complaint of abdominal distension persisting for over 10 days. Her CA125 level was measured at 650 U/mL, and the tumor was classified as stage IIIC. (b) A 70-year-old female patient presented with a complaint of abdominal distension persisting for over one year. Her CA125 level was measured at 457 U/mL, and the tumor was classified as stage III.

2.2.3. Feature extraction

The AK 3.2.0 (Workbench2014, GE Healthcare) was used to extract quantitative radiomic features. This software tool complies with the standards established by the Image Biomarker Standardization Initiative (IBSI) [10]. A total of 2074 radiomic features were extracted from the pre- and post-contrast CT images. These features comprise first-order features, shape, grey-level run-length matrix (GLRLM), grey-level size-zone matrix (GLSZM), grey-level co-occurrence matrix (GLCM), grey-level dependence matrix (GLDM), and neighbourhood grey difference matrix (NGTDM). The image transformation employed logarithmic transformation, parameter Sigma selection 2.0 and 3.0; wavelet transformation, Level 1; local binary mode, Level 2, Radius 1.0, Subdivision select 1.

2.2.4. Feature selection

To ensure that the extracted features are in a consistent and comparable format and facilitate the development of robust and generalisable radiomics models, standardisation of radiomic features is an essential step before feature selection [11]. In this study, we used z-score normalisation to standardise the radiomic features. Subsequently, we leveraged the Least Absolute Shrinkage and Selection Operator (LASSO) algorithm [12] to select a subset of radiomic features that were most informative for predicting PFS from the 2074 pre- and post-contrast CT radiomic features. This algorithm solves an optimisation problem that minimises the sum of the mean-squared errors of the model predictions and a penalty term proportional to the sum of the absolute values of the regression coefficients. The penalty term is controlled by a tuning parameter, denoted as λ (lambda), which determines the amount of shrinkage applied to the coefficients. By varying the value of λ, the LASSO performs a feature selection process, where features with non-zero coefficients are selected as the most relevant ones.

2.2.5. Prognostic model construction

Univariate and multivariate Cox analyses were conducted using stepwise regression to identify independent prognostic indicators. Variables with $P < 0.05$ in both univariate and multivariate analyses were included in the predictive models. The RF algorithm [13] was employed to develop the radiomic and combined models based on the filtered features using four-fold cross-validation, in which three folds (training a stratified four-fold cross-set) were iteratively used to train a model that was subsequently tested on the left-out fold (validation set). The performances of the predictive models were evaluated using metrics such as discrimination, calibration, and clinical validity. The discrimination power was assessed using receiver operating characteristic (ROC) curves. Calibration curves were constructed to assess the goodness of fit between the probabilities predicted by the combined model and the observed event proportions [14]. Clinical validity was evaluated using decision curve analysis (DCA), which quantitatively measures the net benefit of using a particular model in clinical decision-making [15].

2.2.6. Model interpretation and feature importance

The SHAP technique was employed to enhance the interpretability of the combined models at global and local levels, which are typically considered opaque black boxes [16]. SHAP is based on the concept of Shapley values derived from the cooperative game theory. It assigns a value to each feature based on its contribution to prediction when combined with other features. These values represent the average marginal contributions of a feature across all possible feature combinations. Using SHAP values, individual predictions can be explained by attributing the prediction outcome to specific features. The sum of the SHAP values for all features allowed for the decomposition of the model's prediction, enabling a better understanding of the impact of each feature.

2.3. Statistical analysis

When considering sample size for a COX model, it is generally recommended to have at least 10–20 samples per predictor variable. Comparison of clinicopathological features between the training and validation cohorts was performed using a chi-square test or Fisher's exact test (categorical variables), *t*-test or Rank sum test (for continuous variables), where appropriate. The balanced area under the curve (AUC), sensitivity, specificity, positive predictive value (PPV), and negative predictive value (NPV) were computed for the training cohort using the cutoff corresponding to the Youden Index. Since there is no universally accepted criterion for identifying overfitting models, in this analysis, we considered a decrease in performance from the training cohort to the validation cohort of greater than 30 % to be indicative of model overfitting. The Python package (v 3.7.6) was used for all the statistical analyses. A $P < 0.05$ was taken as statistically significant.

3. Results

3.1. Patient characteristics

A total of 102 patients (mean age, 51.6 years ± 10.1) with EOC were included for analysis. Table 1 shows the patient characteristics stratified into the training and validation cohorts. There were no significant differences in clinical variables between the two cohorts (all $p > 0.05$).

3.2. Predictive performance of the radiomic and combined models

After feature selection, one pre-contrast CT feature (original_shape_Sphericity) and three post-contrast CT features (i.e., waveletHLH_glszm_LargeAreaLowGrayLevelEmphasis, waveletLHL_ ngtdm_Busyness, and waveletLLH_gldm_DependenceVariance) were identified using an optimal λ of 0.105 (Fig. 4a and b). The relative feature importance results revealed that waveletHLH_glszm _LargeAreaLowGrayLevelEmphasis and waveletLHL_ngtdm_Busyness were significantly more important than waveletLLH_gldm_DependenceVariance and original_shape_sphericity with relative importance coefficients of 1.000, 0.834, 0.412, and 0.349, respectively. Therefore, we selected the top two radiomic features to construct the radiomic models.

The radiomic model yielded an AUC of 0.762 (95%CI: 0.754–0.770), sensitivity of 0.747 (95%CI: 0.707–0.787), specificity of 0.703 (95%CI: 0.661–0.745), PPV of 0.733 (95%CI: 0.714–0.752), and NPV of 0.735 (95%CI: 0.713–0.757) in the training cohort, and an AUC of 0.713 (95%CI: 0.656–0.770), sensitivity of 0.702 (95%CI: 0.613–0.791), specificity of 0.714 (95%CI: 0.608–0.820), PPV of 0.576 (95%CI: 0.547–0.605), and NPV of 0.639 (95%CI: 0.581–0.697) in the validation cohort.

Multivariate Cox analysis identified venous blood CA125 level ($P = 0.015$), stage III ($P = 0.019$), and Radscore ($P < 0.001$) as independent predictors of PFS (Table 2). Fig. 5a and b shows the predictive performance of the combined model, with a C-index of

Table 1
Patient characteristics in the training and validation cohorts.

Characteristics	Training cohort (n = 77)	Validation cohort (n = 25)	P-value
Age (years)	52.0 ± 9.9	50.3 ± 10.9	0.476
BMI (kg/m^2)	23.0 ± 3.0	22.2 ± 3.6	0.265
FIGO stage			0.838
I	12 (15.6)	5 (20.0)	
II	10 (13.0)	4 (16.0)	
III	48 (62.3)	13 (52.0)	
IV	7 (9.1)	3 (12.0)	
WBC (mm^3)	9.0 ± 4.0	10.2 ± 4.7	0.195
NEU (mm^3)	6.9 ± 4.1	8.2 ± 4.6	0.205
RBC (mm^3)	4.0 ± 0.6	4.0 ± 0.7	0.686
HGB (g/L)	114.9 ± 17.1	108.5 ± 17.4	0.110
PLT (mm^3)	303.6 ± 113.5	326.7 ± 146.7	0.414
Venous blood CA125 (U/mL)	1302.2 ± 1871.1	1291.4 ± 2674.3	0.982
Whole boold CA125 (U/mL)	383.1 ± 290.0	470.4 ± 467.6	0.269
Median PFS (months)	41.1 ± 26.9	45.6 ± 31.8	0.489

Abbreviations: BMI, Body mass index; WBC, White blood cells; NEU, Neutrophil; RBC, Red blood cells; HGB, Hemoglobin; CA125, Carbohydrate antigen 125; PFS, Progression-free survival.

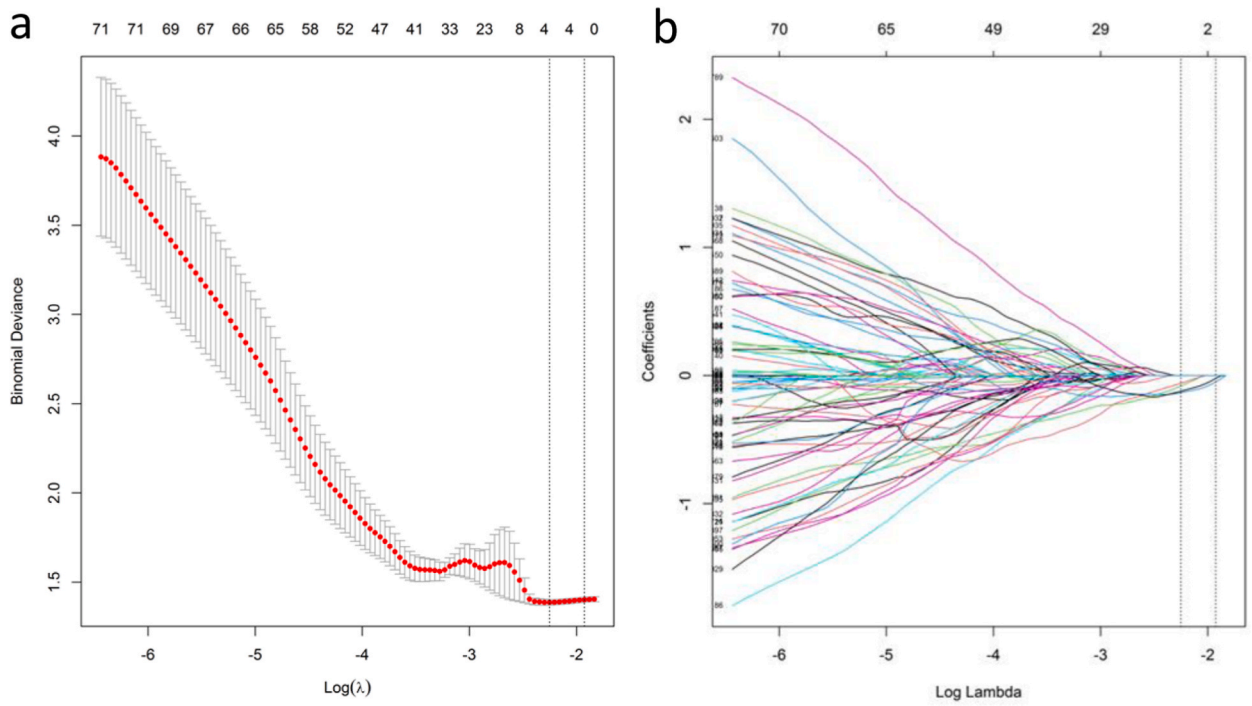

Fig. 4. Radiomics feature selection with the least absolute shrinkage and selection operator (LASSO) binary logistic regression model. (a) Tuning parameter (l) selection in the LASSO model used four-fold cross-validation with minimum criteria. Left vertical lines indicate the optimal value of the LASSO tuning parameter (λ). (b) LASSO coefficient profile plot with different log (λ). Vertical dashed lines represent four radiomic features with nonzero coefficients selected with the optimal λ value.

0.745 (95%CI: 0.678–0.812). For predicting 3-year PFS, the combined model achieved an AUC of 0.812 (95%CI: 0.802–0.822), sensitivity of 0.803 (95%CI: 0.766–0.840), specificity of 0.703 (95%CI: 0.659–0.747), PPV of 0.768 (95%CI: 0.744–0.792), and NPV of 0.769 (95%CI: 0.751–0.787) in the training cohort and an AUC of 0.772 (95%CI: 0.732–0.812), sensitivity of 0.734 (95%CI: 0.657–0.811), specificity of 0.688 (95%CI: 0.666–0.710), PPV of 0.609 (95%CI: 0.574–0.644), and NPV of 0.690 (95%CI: 0.615–0.765) in the validation cohort.

The calibration curves (Fig. 5c) exhibited a high concordance level between the predicted and actual observed probabilities (Hosmer–Lemeshow test, P = 0.179). DCA (Fig. 5d) showed high clinical applicability for the combined model with a wide range of threshold probabilities (5–85 %).

Table 2
Multivariate Cox proportional hazards analysis of clinical variables and radiomic signature.

Predictors	Estimate	Standard error	Z	P-value	Hazard Ratio	Lower	Upper
Age	0.007	0.014	0.465	0.642	1.007	0.979	1.036
BMI	0.017	0.051	0.326	0.744	1.017	0.92	1.124
Tumor stage							
Stage I	Ref.						
Stage II	1.337	0.735	1.82	0.069	3.809	0.902	16.079
Stage III	1.553	0.665	2.336	**0.019**	4.724	1.284	17.375
Stage IV	1.449	0.771	1.879	0.060	4.259	0.940	19.306
WBC	−0.067	0.206	−0.325	0.745	0.935	0.624	1.401
NEU	0.123	0.218	0.565	0.572	1.131	0.738	1.735
RBC	0.17	0.469	0.363	0.717	1.185	0.473	2.970
HGB	−0.001	0.016	−0.034	0.973	0.999	0.969	1.031
Platelet	0.002	0.001	1.447	0.148	1.002	0.999	1.005
Venous blood CA125	−0.002	0.001	−2.437	**0.015**	0.998	0.997	1
Whole boold CA125	0	0	0.538	0.590	1	1	1
Radscore	0.116	0.032	3.573	**<0.001**	1.123	1.054	1.197

Abbreviations: BMI, Body mass index; WBC, White blood cells; NEU, Neutrophil; RBC, Red blood cells; HGB, Hemoglobin; CA125, Carbohydrate antigen 125.

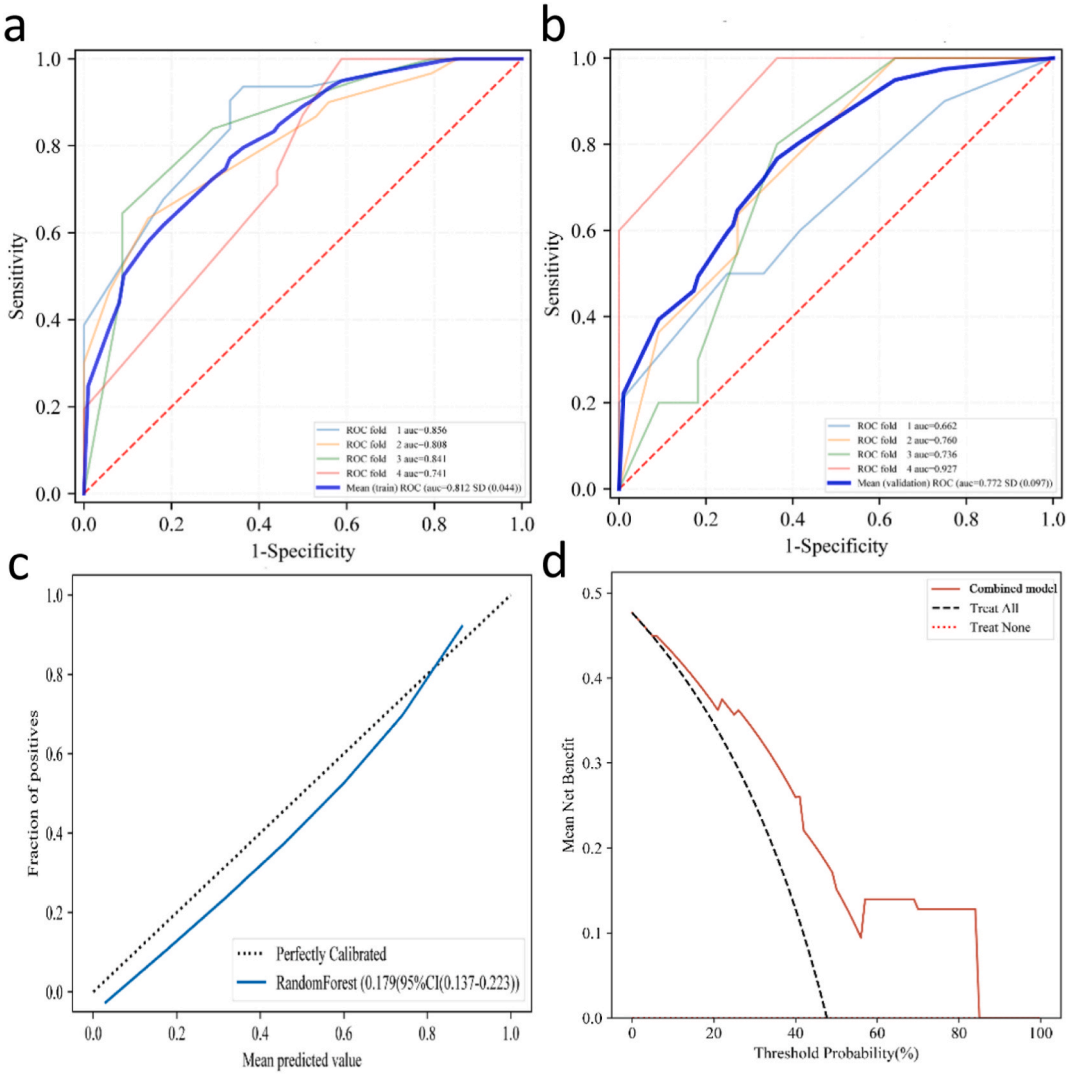

Fig. 5. Predictive performance of the combined model. (a–b) Receiver operator characteristic curve in the training and validation cohorts; (c) Calibration curve; (d) Clinical decision curve.

3.3. Interpretability of the combined model

The SHAP feature importance plots revealed that the Radscore had the highest importance in the combined model, followed by tumour stage and venous blood CA125. The plots show the distribution of the Shapley values for each feature, suggesting their impact on the model output. A higher SHAP value for a feature indicated a greater probability of disease progression. The summary plot demonstrates the relationship between a feature's SHAP value and its influence on the model prediction. Fig. 6a–d shows the SHAP explanatory force plots for the two representative cases, illustrating how the features push the model's output away from the baseline.

4. Discussion

In this study, we developed a radiomics model to predict EOC prognosis based on quantitative radiomics features and clinical information using the RF algorithm. The results demonstrated that the Radscore could significantly increase the accuracy of clinical variables (such as the FIGO stage and venous blood CA125). In addition, we leverage the SHAP method to display the relative importance of significant features and attribute the contribution of each feature to the final prediction. This approach allows users to gain insight into the decision-making process and build trust in the model's predictions.

EOC is a prevalent and highly lethal disease characterised by high mortality rates [17]. It is of the utmost importance to develop accurate prognostic tools and personalised therapeutic strategies to enhance patient outcomes. In our study, we focused on utilising high-dimensional radiomic features extracted from the entire tumour volume, as opposed to a single slice, to better capture the

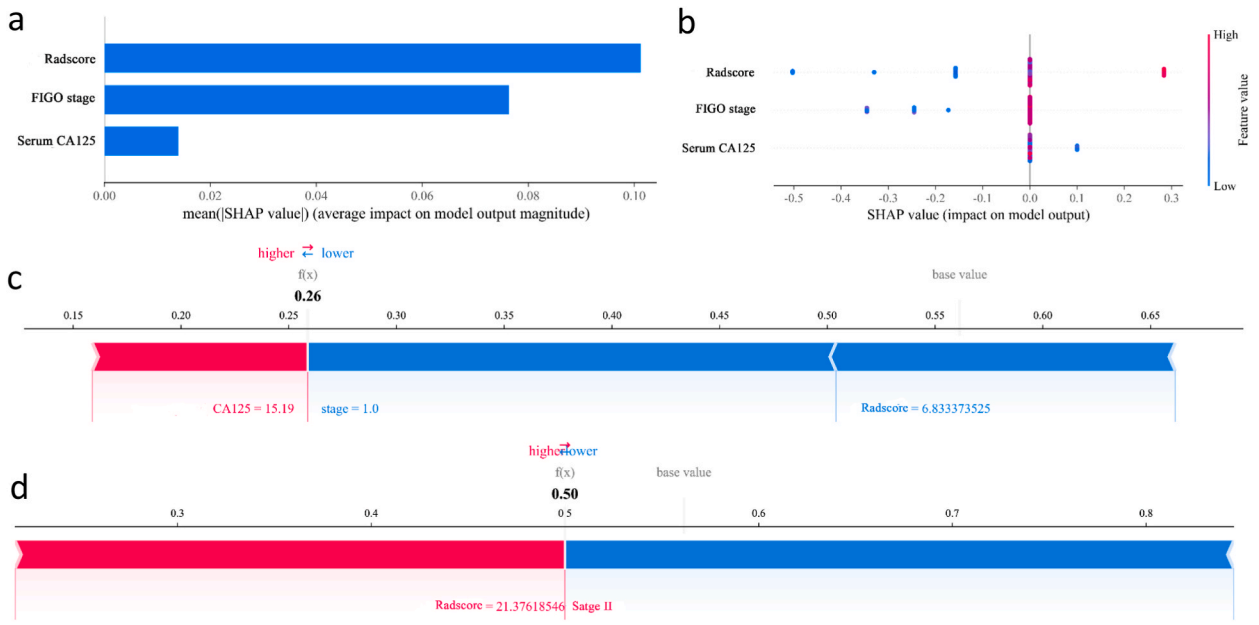

Fig. 6. Global and individual interpretation of the combined model using SHAP method. (a–b) SHAP feature importance and summary plots; (b–d) The SHAP local force plots for two representative cases.

intrinsic characteristics of EOC. Feature selection is also a crucial step in radiomics analysis as it helps identify the most relevant and informative features for predicting outcomes. During the building of the radiomic signature, the LASSO method was applied to remove highly correlated radiomic features, including those that exhibited high correlations with the volume/voxel [18]. After feature selection, four radiomic features were identified: one shape and three wavelet-transformed texture features. Unlike previous studies, our study further ranked the relative importance of the selected features within the RF model. Two wavelet features with the most significant impact on model prediction were identified. These two features measure the variation in grey-level intensity within the voxel neighbourhood in the image and the distribution of large homogeneous areas based on their size and grey-level intensity, respectively [19]. Wavelet-transformed features can capture variations in texture patterns at various scales and orientations, providing valuable information about tumour heterogeneity, which dictates the treatment response and prognosis.

To enhance the accuracy of survival prediction, clinical factors were incorporated into the radiomics signature to develop a comprehensive model. The clinical radiomics model showed acceptable discrimination. Notably, the radiomic signature provides additional value beyond the traditional FIGO staging system. Thus, the combined model can be considered a reliable tool for estimating the postoperative survival of patients with EOC. Although multiple previous studies [20–27] have been developed to predict the survival outcomes of patients with EOC, their models lacked interpretability, which limited clinical transformation. In this study, the SHAP algorithm was used to identify the most important features contributing to the model's predictive performance. The results showed that Radsocre was the most important feature, followed by FIGO stage and venous blood CA125 levels. The SHAP algorithm provides a transparent and interpretable method for communicating the model's predictions to clinicians and patients. It generates feature importance plots that visually represent the contribution of each radiomic feature to the model's predictions [28]. This enhances the trust and acceptance of the model in clinical settings because clinicians can easily grasp the underlying rationale behind the predictions.

This study had some limitations. First, the retrospective design introduces inherent limitations, such as reliance on existing medical records and the potential for incomplete or missing data. This may have affected the accuracy and reliability of our findings. Additionally, the retrospective nature of the study may introduce a selection bias, as the study population was based on patients who had already been diagnosed with EOC and underwent CT scans. This may limit the generalisability of our results to other populations and settings. Second, the relatively small sample size may limit the generalisability of the findings, which has been a challenge in previous studies. However, a held-out validation was performed to mitigate bias and obtain more robust results. Third, our radiomics features were extracted from CT images; features from other modalities, such as MRI, may provide different information regarding tumour heterogeneity. Fifth, the biological interpretation of radiomic features remains a challenging issue and requires further investigation [29,30]. Exploring associations with digital pathology features, conducting radiology-pathology co-registration, and assessing biological pathways or genomic correlations can provide valuable insights into the underlying biology and mechanisms driving the observed radiomic patterns [31]. Finally, an external validation of the acquired data is necessary to confirm the reliability and reproducibility of the findings. Future studies should aim to validate these results using independent datasets to ensure the generalisability of radiomic models.

5. Conclusions

Our study demonstrated that the RF model can potentially assess prognostic risk in patients with EOC. The radiomics-based model, which includes the FIGO stage, venous blood CA125 level, and Radscore, offers a noninvasive approach to predicting survival outcomes. This model can potentially contribute to the field of precision medicine for EOC, fulfilling the ultimate goal of personalised treatment of patients.

Availability of data and materials

Data and material are available from the corresponding author upon request.

CRediT authorship contribution statement

Lian Jian: Writing – review & editing, Writing – original draft, Project administration, Investigation, Conceptualization. **Xiaoyan Chen:** Writing – review & editing, Project administration, Investigation, Data curation. **Pingsheng Hu:** Formal analysis, Data curation. **Handong Li:** Writing – review & editing, Data curation. **Chao Fang:** Writing – review & editing, Data curation. **Jing Wang:** Writing – review & editing, Resources. **Nayiyuan Wu:** Writing – review & editing, Visualization, Validation, Supervision, Resources, Conceptualization. **Xiaoping Yu:** Writing – review & editing, Validation, Supervision, Resources, Conceptualization.

Declaration of competing interest

The authors declare that they have no known competing financial interests or personal relationships that could have appeared to influence the work reported in this paper.

Acknowledgements

We would like to thank Editage (www.editage.com) for English language editing.

References

[1] H. Sung, J. Ferlay, R.L. Siegel, et al., Global cancer statistics 2020: GLOBOCAN estimates of incidence and mortality worldwide for 36 cancers in 185 Countries, CA Cancer J Clin 71 (2021) 209–249.
[2] S. Lheureux, C. Gourley, I. Vergote, et al., Epithelial ovarian cancer, Lancet 393 (2019) 1240–1253.
[3] S.B. Elsherif, P.R. Bhosale, C. Lall, et al., Current update on malignant epithelial ovarian tumors, Abdom Radiol (NY) 46 (2021) 2264–2280.
[4] M.E. Mayerhoefer, A. Materka, G. Langs, et al., Introduction to radiomics, J. Nucl. Med. 61 (2020) 488–495.
[5] P. Lambin, R.T.H. Leijenaar, T.M. Deist, et al., Radiomics: the bridge between medical imaging and personalized medicine, Nat. Rev. Clin. Oncol. 14 (2017) 749–762.
[6] G. Singh, S. Manjila, N. Sakla, et al., Radiomics and radiogenomics in gliomas: a contemporary update, Br. J. Cancer 125 (2021) 641–657.
[7] M. Akazawa, K. Hashimoto, Artificial intelligence in gynecologic cancers: current status and future challenges - a systematic review, Artif. Intell. Med. 120 (2021) 102164.
[8] Z. Jin, S. Pei, L. Ouyang, et al., Thy-Wise: an interpretable machine learning model for the evaluation of thyroid nodules, Int. J. Cancer 151 (2022) 2229–2243.
[9] M. Kokla, J. Virtanen, M. Kolehmainen, et al., Random forest-based imputation outperforms other methods for imputing LC-MS metabolomics data: a comparative study, BMC Bioinf. 20 (2019) 492.
[10] A. Zwanenburg, M. Vallières, M.A. Abdalah, et al., The image biomarker standardization initiative: standardized quantitative radiomics for high-throughput image-based phenotyping, Radiology 295 (2020) 328–338.
[11] Y. Zhang, S. Yu, L. Zhang, et al., Radiomics based on CECT in differentiating Kimura disease from lymph node metastases in head and neck: a non-invasive and reliable method, Front. Oncol. 10 (2020) 1121.
[12] B. Zhang, J. Tian, D. Dong, et al., Radiomics features of multiparametric MRI as novel prognostic factors in advanced nasopharyngeal carcinoma, Clin. Cancer Res. 23 (2017) 4259–4269.
[13] B. Zhang, X. He, F. Ouyang, et al., Radiomic machine-learning classifiers for prognostic biomarkers of advanced nasopharyngeal carcinoma, Cancer Lett. 403 (2017) 21–27.
[14] A.A. Kramer, J.E. Zimmerman, Assessing the calibration of mortality benchmarks in critical care: the Hosmer-Lemeshow test revisited, Crit. Care Med. 35 (2007) 2052–2056.
[15] B. Van Calster, L. Wynants, J.F.M. Verbeek, et al., Reporting and interpreting decision curve analysis: a guide for investigators, Eur. Urol. 74 (2018) 796–804.
[16] S.M. Lundberg, S.-I. Lee, A unified approach to interpreting model predictions, in: 31st Conference on Neural Information Processing Systems (NIPS 2017), 2017. Long Beach, CA, USA.
[17] S.B. Elsherif, P.R. Bhosale, C. Lall, et al., Current update on malignant epithelial ovarian tumors, Abdom Radiol (NY) 46 (2021) 2264–2280.
[18] C. Fotopoulou, A. Rockall, H. Lu, et al., Validation analysis of the novel imaging-based prognostic radiomic signature in patients undergoing primary surgery for advanced high-grade serous ovarian cancer (HGSOC), Br. J. Cancer 126 (2022) 1047–1054.
[19] F. Davnall, C.S. Yip, G. Ljungqvist, et al., Assessment of tumor heterogeneity: an emerging imaging tool for clinical practice? Insights Imaging 3 (2012) 573–589.
[20] F. Zhan, L. He, Y. Yu, et al., A multimodal radiomic machine learning approach to predict the LCK expression and clinical prognosis in high-grade serous ovarian cancer, Sci. Rep. 13 (2023) 16397.
[21] R. Gu, S. Tan, Y. Xu, et al., CT radiomics prediction of CXCL9 expression and survival in ovarian cancer, J. Ovarian Res. 16 (2023) 180.
[22] S. Wan, T. Zhou, R. Che, et al., CT-based machine learning radiomics predicts CCR5 expression level and survival in ovarian cancer, J. Ovarian Res. 16 (2023) 1.
[23] L. Gao, W. Jiang, Q. Yue, et al., Radiomic model to predict the expression of PD-1 and overall survival of patients with ovarian cancer, Int. Immunopharm. 113 (2022) 109335.
[24] Y. Zheng, F. Wang, W. Zhang, et al., Preoperative CT-based deep learning model for predicting overall survival in patients with high-grade serous ovarian cancer, Front. Oncol. 12 (2022) 986089.
[25] J. Hu, Z. Wang, R. Zuo, et al., Development of survival predictors for high-grade serous ovarian cancer based on stable radiomic features from computed tomography images, iScience 25 (2022) 104628.

[26] F. Yao, J. Ding, Z. Hu, et al., Ultrasound-based radiomics score: a potential biomarker for the prediction of progression-free survival in ovarian epithelial cancer, Abdom Radiol (NY) 46 (2021) 4936–4945.
[27] S. Wang, Z. Liu, Y. Rong, et al., Deep learning provides a new computed tomography-based prognostic biomarker for recurrence prediction in high-grade serous ovarian cancer, Radiother. Oncol. 132 (2019) 171–177.
[28] C. Ladbury, R. Zarinshenas, H. Semwal, et al., Utilization of model-agnostic explainable artificial intelligence frameworks in oncology: a narrative review, Transl. Cancer Res. 11 (2022) 3853–3868.
[29] M.R. Tomaszewski, R.J. Gillies, The biological meaning of radiomic features, Radiology 298 (2021) 505–516.
[30] Q. Sun, Y. Chen, C. Liang, et al., Biologic pathways underlying prognostic radiomics phenotypes from paired MRI and RNA sequencing in glioblastoma, Radiology 301 (2021) 654–663.
[31] L. Zhang, J. Zheng, Z. Jin, et al., The potential and challenges of radiomics in uncovering prognostic and molecular differences in interstitial lung disease associated with systemic sclerosis, Eur. Respir. J. 59 (2022) 2102792.